Electronic Supplementary Material (ESI) for Nanoscale Advances.

Exosomes trapping, manipulation and size-based separation using opto-thermo-electrohydrodynamic tweezers

Chuchuan Hong1,2, Sen Yang2,3, Justus Ndukaife1,2

1. Electrical and computer engineering department, Vanderbilt University, Nashville, TN, 37212, USA
2. Vanderbilt Institute of Nanoscale Science and Engineering, Vanderbilt University, Nashville, TN, 37212, USA
3. Interdisciplinary Material Science, Vanderbilt University, Nashville, TN, 37212, USA

1. Thermal and microfluidic simulation

The power dissipation density in the gold film on glass substrate is modeled using equation (1) shown below in COMSOL Multiphysics. Model takes into account the Gaussian distribution of the incident laser beam and exponential decay of light in the gold film.

$$Q(r) = P_0 A \frac{\alpha_{Au}}{\pi\sigma^2} e^{-\left(\frac{x^2+y^2}{2\sigma^2}\right)} e^{-\alpha_{Au} z} \quad (1)$$

,where P_0 is incident laser power, A is the absorption of the nanohole array. The attenuation coefficient in the nanohole array at the illumination wavelength is given by $\alpha_{Au} = \frac{4\pi\kappa}{\lambda} = 8.91 \times 10^7\ m^{-1}$, where κ is the imaginary part of the refractive index of gold.

The temperature distribution under laser is obtained by solving the heat conduction equation given by:

$$-k\nabla^2 T + \rho C_p u \cdot \nabla T = Q \quad (2)$$

k is the thermal conductivity of the materials (glass, sapphire, gold, or water). T is the temperature in Kelvin, and ∇T is the temperature gradient. The second term is the convection term, which depends on u, the velocity of the fluid. For the chamber height in our case, 120 µm, the convection term can be neglected [1,2]. ρ is the density of the fluid and C_p is the specific heat capacity at constant pressure. Q is the heat source density, which is calculated from equation (1). The outer temperature on the outer surface of the boundaries was set to $T = 293.15\ K$.

After the thermal simulation, we solved the Poisson equation below to calculate the electric field applied:

$$\nabla \cdot E = \frac{\rho}{\varepsilon_0}, \text{ with } E = -\nabla V \quad (3)$$

The calculated electric field distribution is imported into the microfluidic model for ETP and ACEO simulation.

Firstly, the ACEO flow is obtained by simulating laminar flow module by defining a slip boundary condition given by the Smoluchowski slip velocity around the nanohole array.

The Smoluchowski slip velocity $\vec{u}$ is given by: $\vec{u} = \mu_{eo}\vec{E}_t$, where $\mu_{eo} = -\frac{\varepsilon_r \varepsilon_0 \zeta}{\mu}$ is the electroosmotic mobility, ε_r is the relative permittivity, ε_0 is the permittivity of free-space, ζ is the zeta potential of the electrical double layer at the nanohole array and fluid interface, and μ is the dynamic viscosity of the liquid. $\vec{E}_t = \vec{E} - (\vec{E} \cdot \vec{n})\vec{n}$ is the tangential component of the electric field, where $\vec{E}$ is calculated by solving equation 3.

The zeta potential here is considered increasing as a.c. frequency drops. Hence, the ACEO flow is stronger as lower a.c. frequency so that it boosts the trapping stability. A more detailed description on the analysis of ACEO flow versus a.c. frequency can be found in our previously reported document [1,3].

Secondly, the ETP flow arise from the localized heating of the fluid to establish a gradient in the permittivity and electrical conductivity in an applied a.c. electric field. The volumetric body force induced in the fluid known as the electrothermal force density, f_{ET} is given by [4]:

$$f_{ET} = \rho_e E - \frac{1}{2}|E|^2 \nabla \varepsilon_m \tag{4}.$$

After perturbative expansion in the limit of small temperature gradient, the force density is derived into [5]:

$$f_{ET} = \frac{1}{2} Re\{\frac{\varepsilon(\alpha - \beta)(\nabla T.E)E^*}{\sigma + i\omega\varepsilon} + \frac{1}{2}\varepsilon\alpha|E|^2\nabla T\} \tag{5}$$

,where $\alpha = {}^{1}\!/_{\varepsilon}\frac{\partial \varepsilon}{\partial T} = -0.004\ K^{-1}$ and $\beta = {}^{1}\!/_{\sigma}\frac{\partial \sigma}{\partial T} = 0.02\ K^{-1}$. ε and σ stands for the permittivity and conductivity of the fluid, respectively. ω is the a.c. field frequency, while ∇T is the temperature gradient calculated from solving the heat equation stated in equation (2).

Lastly, we solved the Navier-Stokes equation using laminar flow module in COMSOL Multiphysics to find out the velocity:

$$\rho_0[u(r) \cdot \nabla]u(r) + \nabla p(r) - \eta\nabla^2 u(r) = F \tag{6},$$

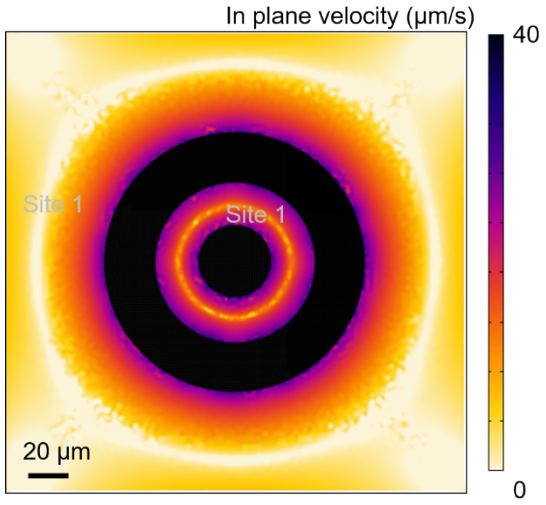

Figure S1: the colormap shows the two stagnations zones created by the electrohydrodynamic flows, where the in-plane velocity drops to zero.

2. Trapping stability under various experimental conditions

As a supplementary of Fig 3. (d) and (e) in the main manuscript, the azimuthal direction stability of trapped smaller exosomes in site I or II and the azimuthal stability of different sizes exosomes are provided in Fig S2 (a) and (b), respectively. The azimuthal angle is defined as the angle θ as shown in Fig S2 (c), where the two dotted lines indicate the particle trajectory. It shows for either site I or II, as well as small or large exosomes, the angle where the trapped exosomes sweep along azimuthal direction does not differ significantly. However, as the exosome is closer to the center of pattern, which is at site II, the absolute distance exosomes cover is shorter. Hence, site I does provide a better spatial confinement along azimuthal direction.

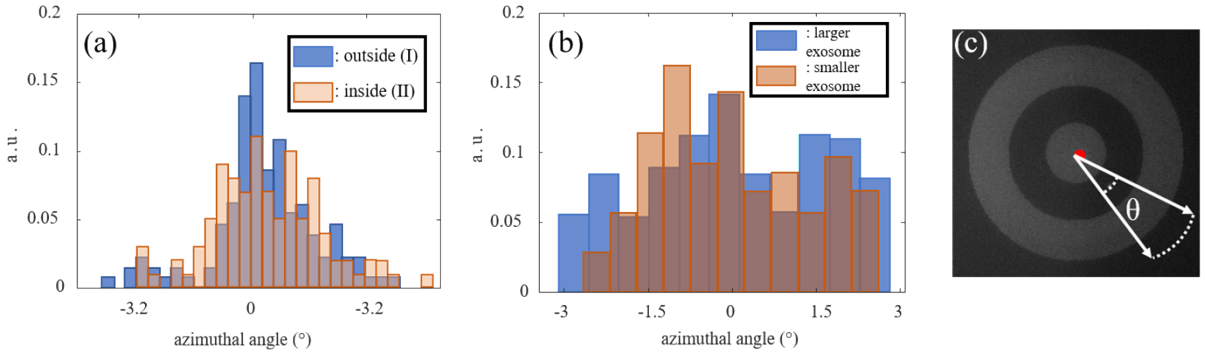

Figure S2: (a) Histograms of azimuthal angle shifts from the same small size exosome on site I or II. (b) Histograms of azimuthal angle shifts from exosomes of different sizes on site II. (c) Definition of azimuthal angle θ.

Additionally, we investigate the trapping stability versus a.c. frequency or the gap size in site II. Results are provided below in Fig S3 and S4. Fig S3 plots out the radial position shift (left column) and azimuthal angle distribution (right column), respectively, under various a.c. frequency from the same small exosome

at site II. It clearly shows the trapping stability is enhanced as a.c. frequency is tuned down from 3.5 kHz to 1.5 kHz. We ascribe this enhancement to the stronger ACEO flow from nanohole arrays from both sides in site II. Fig S4 depicts the trapping stability with various gap size in site II. As gap size is tuned down from 20 µm to 6 µm, under 3 kHz a.c. frequency, we found the trapping stability is strengthened along radial direction but weakened along azimuthal direction. This discovery can be utilized to further optimize our CNA system.

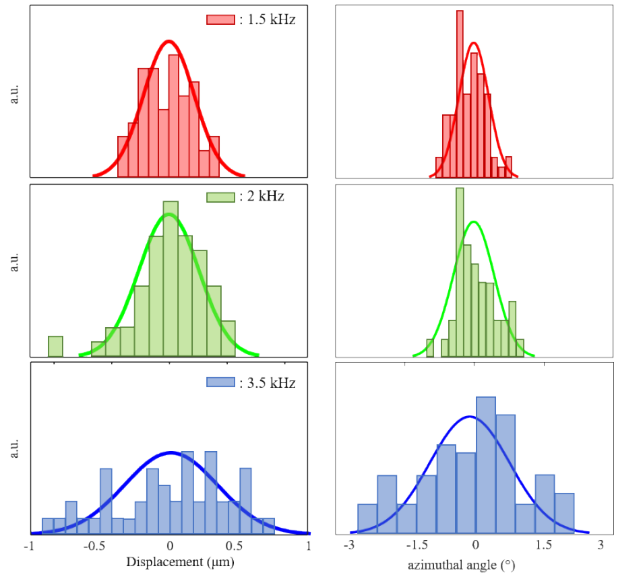

Figure S3: Histograms of radial displacement and azimuthal angle shifts from the same small size exosome under various a.c. frequency, on site I.

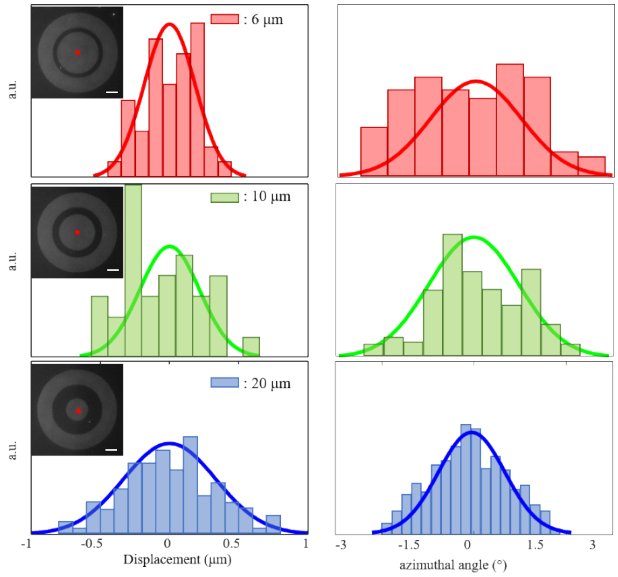

Figure S4: Histograms of radial displacement and azimuthal angle shifts of trapped single exosome in site I of different gap sizes. Insets are images capture by camera to illustrate the size of pattern and gap width. Scalebar represents 20 µm.

3. Fabrication process

In this fabrication, we adapted the template strip method mentioned in ref [6]. Starting from a bare silicon wafer, a 10 nm Cr mask was thermally evaporated serving as hard mask. We then spincoated PMMA A4 and patterned the nanohole array through e-beam lithography. After exposure and development, an oxygen descum step followed up immediately before Cr wet etch. The sample was soaked in Cr etchant for 10 seconds and rinsed thoroughly by deionized water. The pattern was thus transferred to Cr hard mask. A one minute reactive ion etch was subsequently carried out to open holes into Si wafer as deep as 500 nm, at least. To finalize the Si template, we cleaned the sample surface by oxygen plasma for 5 minutes and stripped off Cr hard mask using Cr etchant. The gold film of 120 nm was then directly evaporated on the Si template, without adhesion layer. Since the depth of hole, ~500 nm, is much greater than the thickness of gold film, the gold falling onto nanoholes would finally sit at the bottom of them, disconnected from the main gold film on the top of Si template. Therefore, we have the CNA patterned into gold film. The final step was to use UV epoxy to transfer the gold film onto a glass substrate.

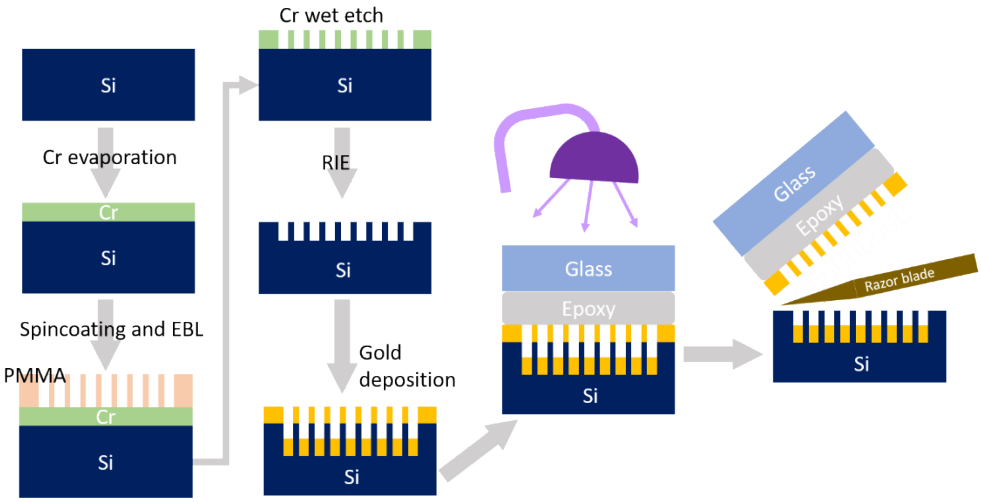

Figure S5: fabrication flow graph showing the steps to make silicon template and template-strip.

Supplementary Movies:

Movie1: trap and sort of exosomes. Beginning with low a.c. frequency, individual exosomes are rapidly transported by ETP and trapped in site II. The a.c. frequency is tuned up to 3.5 kHz and we observe the two smaller exosomes hop into site I, while larger exosomes stay outside. Then, a.c. frequency is tuned down to 2 kHz to stabilize all trapped exosome and no further relocation is observed.

Movie2: dynamic manipulation of trapped exosome in site I using laser motion. The laser was moving in a circle across the center nanohole array with the trapped small exosome moving following the motion of laser. The trapped large exosome on site II stay to the right-top corner of the CNA pattern during the laser motion.

(1) Hong, C.; Yang, S.; Ndukaife, J. C. Stand-off Trapping and Manipulation of Sub-10 Nm Objects and Biomolecules Using Opto-Thermo-Electrohydrodynamic Tweezers. *Nature Nanotechnology* **2020**, *15* (11), 908–913. https://doi.org/10.1038/s41565-020-0760-z.

(2) Ndukaife, J. C.; Kildishev, A. v.; Nnanna, A. G. A.; Shalaev, V. M.; Wereley, S. T.; Boltasseva, A. Long-Range and Rapid Transport of Individual Nano-Objects by a Hybrid Electrothermoplasmonic Nanotweezer. *Nature Nanotechnology* **2016**, *11* (1), 53–59. https://doi.org/10.1038/nnano.2015.248.

(3) Hwang, H.; Park, J.-K. Rapid and Selective Concentration of Microparticles in an Optoelectrofluidic Platform. *Lab Chip* **2009**, *9* (2), 199–206. https://doi.org/10.1039/B811740C.

(4) Melcher, J. R.; Firebaugh, M. S. Traveling-Wave Bulk Electroconvection Induced across a Temperature Gradient. *Physics of Fluids* **1967**. https://doi.org/10.1063/1.1762260.

(5) Ramos, A.; Morgan, H.; Green, N. G.; Castellanos, A. Ac Electrokinetics: A Review of Forces in Microelectrode Structures. *Journal of Physics D: Applied Physics* **1998**, *31* (18), 2338–2353. https://doi.org/10.1088/0022-3727/31/18/021.

(6) Treml, B. Template Stripping for High Throughput Fabrication of Nanohole Arrays. **2010**.